Chapter 5: Study of photo-electrochemical property of pure and ZnO-BiVO4 photoanodes

5.1 Set-up for photo-electrochemical study

All Photoelectrochemical measurements (photocurrent, EIS, Mott-Schottky) were carried out with Solartron Cell Test System (Model 1470E 8 Channel Potentiostat/Galvanostat combined with Model 1400A Chassis). Three electrode systems were used consisting of $BiVO_4$/ZnO (photoanode), platinum wire (cathode) Ag/AgCl (reference) and 1 M NaOH(electrolyte). Samples were dipped in electrolyte for 10 min for charge carrier stabilization before measurements. Current-time curves were taken with 0 applied potential. Current-voltage curves were taken from -1.2V to +1.2 V with scan rate of 50 mV/s. Mott-Schottky measurements (or step potential impedance) were taken in the range -1 to 0V at1000 Hz. These curves were used to calculate the charge carrier density (N_D) and flat band potential (V_{FB}) using slope and intercept, respectively. For Nyquist curves, Ac impedance measurements were carried out in a frequency range 0.1 Hz to 106 Hz at 0 V potential. These curves were used to measure the charge transfer resistance of the samples. All the electrochemical measurements were carried out in dark as well as illumination condition by simulated sun light form Xenon arc lamp with AM 1.5 with power 100 mW/cm^2. The electrodes with exposed area of 1cm x 1cm were subjected to chopped light with an interval of 10 sec from the front side.

5.2 Result and discussion

The photoelectrochemical process is studied on four photoanode samples ZnO, B1 (0.038 M $BiVO_4$/ZnO), B2 (0.05 M $BiVO_4$/ZnO) and B3 (0.1 M $BiVO_4$/ZnO). Figure 5.1 shows the

photocurrent response as a function of time for samples ZnO, B1, B2 and B3 under illumination. The sample B1 had shown maximum photocurrent density of 13.5 x 10^{-4}A/cm^2 which is significantly higher than those from the bare ZnO (6.0 x 10^{-4} A/cm^2) electrode upon illumination. The enhanced photo response of B1 photoanode is attributed to (i) extended photo response to the visible region as $BiVO_4$ is a visible light driven photocatalyst and (ii) suitable flat band positions involving electron transfer from $BiVO_4$ to ZnO, thus enhancing the charge separation [13,216]. The flat band potential mechanism is of significant importance to improve the solar to hydrogen efficiency (SHE). Figure 5.5 shows the schematic diagram to illustrate electron transfer from $BiVO_4$ (low CB edge material) to ZnO (high CB edge material) by almost matching flat band potential phenomenon. Thus unusual charge transfer from low CB edge material to high CB edge material is of paramount importance in $BiVO_4/TiO_2$ and $BiVO_4$/ZnO hetrojunction based photoanode systems resulting in prolonged lifetime of charge carriers to promote charge separation. Otherwise, in pure $BiVO_4$, the high energy electron usually relax to the bottom of CB quickly rather than participating in reduction reactions.

The mole ratio of ZnO and $BiVO_4$ in ZnO/$BiVO_4$ greatly affects its photoactivity. Increase in content of $BiVO_4$ from sample B1 to B3, causes reduction in photoactivity from B1 to B3. This is due to the suppression of effective charge separation and increase in photogenerated electron–hole pair recombination at the hetrojunction by suitable content ratio of composite components.

Since we are depositing $BiVO_4$ in the layer form, which means varying the content of $BiVO_4$ in composite will vary the thickness of the deposited $BiVO_4$ layer on ZnO, which is a deciding factor for the available charge density for photoreactions in ZnO and recombination rate at the interface. Upon illumination, electrons in $BiVO_4$ near the interface are extracted and transferred to ZnO conduction band. Now on moving from sample B1 to B3, thickness of $BiVO_4$ layer increases. It's been well reported that on increasing the layer thickness reduces the extraction of charge carriers by elevating the time duration of charge transfer and further it increases the bulk

recombination rate of charge carriers. So in sample B2 and B3, at the instant of beginning of illumination period, surface electrons in $BiVO_4$ near interface are immediately extracted to ZnO resulting in increase in photocurrent but after some time recombination rate within bulk $BiVO_4$ layer dominates extraction rate of electrons which leads to sudden drop in photocurrent resulting in the formation of spike as shown in figure 5.1.

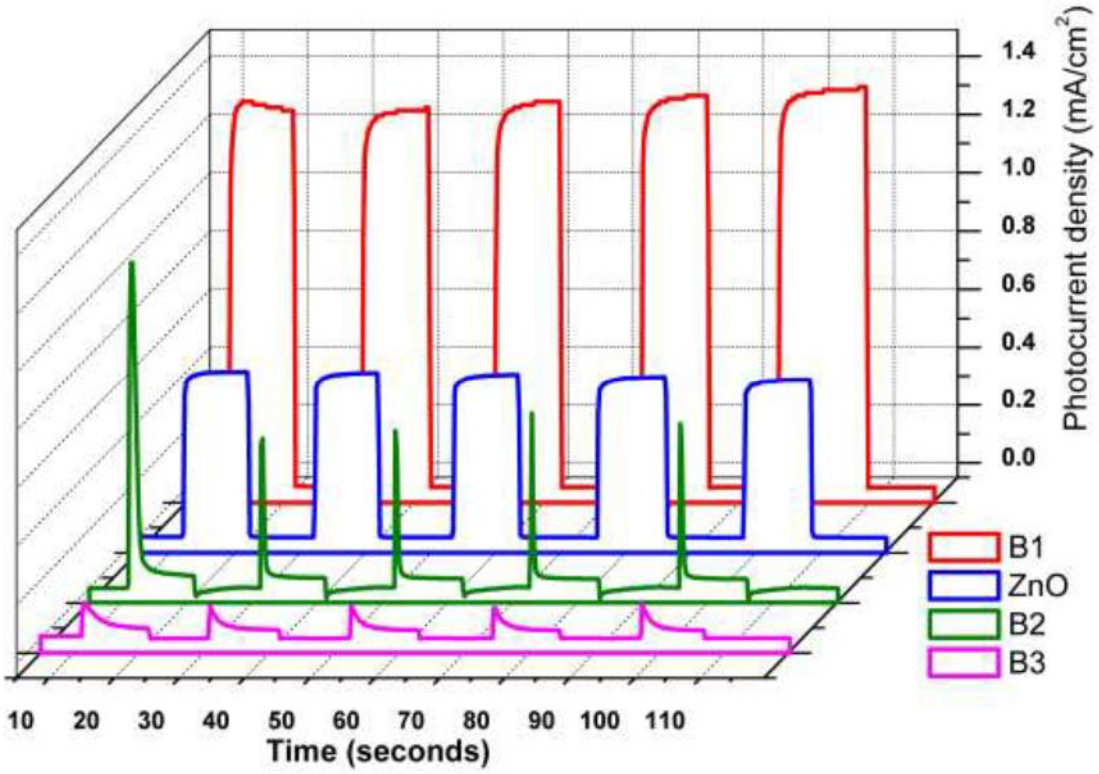

Figure 5.1 Photocurrent-time characteristics (J vs t) of photoanode samples (a) pure ZnO (b) B1;$BiVO_4$ (0.035 M)/ZnO (c) B2;$BiVO_4$ (0.05 M)/ ZnO and (d) B3;$BiVO_4$ (0.1M)/ ZnOat applied potential 0 V in 1 M NaOH light source having 300-500 nm wavelength at 1 sun intensity.

The photoresponse curve shows significant impact of $BiVO_4$ concentration on the current-time characteristics as shown (Fig 5.1), the photoresponse of sample B2 and B3 is characterized by 'spike and overshoot' features. In sample B2, upon illumination the current density is increased to ~5.5 x 10^{-4} A/ cm^2 (spike feature) and then sharply and drastically reduces to ~5.8 x 10^{-5} A/ cm^2

within fractions of seconds. The increase in photocurrent density upon illumination 'overshoot feature' is attributed to the excitation of electrons to the conduction band and rapid decrease in photocurrent density 'decay feature' is due to the (i) higher recombination rate of electron-hole pair and (ii) slow transfer rate of the electrons [17]. The kinetic competition between water oxidation and electron-hole recombination give rise to overshoot feature in photocurrent curve. The similar spike and overshoot features are observed in photoresponse curve of hematite based photoanodes [15,16]. There was no such decrease in the photocurrent response of sample B1 was observed because the recombination rate is low due to the lower $BiVO_4$ concentration. As the generation of electron-hole pair is faster than the transfer rate of holes and electrons, holes get accumulated at the surface. When the illumination was stopped, these holes trapped at the surface recombine with the electrons, thus giving a current in the negative direction, also known as 'back current'. In summary, spike feature and overshoot feature are attributed to two recombination processes, (i) rapid electron-hole recombination and (ii) surface-accumulated holes and $BiVO_4$ electrons recombination, respectively. These two 'surface recombination' processes in $BiVO_4$ photoanode limits the solar to hydrogen efficiency (SHE) and results in current spikes at potentials near the onset of photocurrent generation. The photocurrent density becomes worse in sample $BiVO_4$, decrease to10 fold times as observed in sample B1. The overall, photocurrent density is found to be decrease in B2 and B3 photoanode with respect to B1 and bare ZnO. Thus increased $BiVO_4$ concentration in sample B3, results in substantially enhanced recombination rate of electron-hole leading to poor photocurrent response. Thus, poor photo response observed in sample B2 and B3 is attributed to excessive electron-hole recombination, low mobility and short diffusion length of photo generated charge carriers and slow water oxidation kinetics of $BiVO_4$ [12, 17]. Thus, photocurrent response observed in $BiVO_4$/ZnO photoanode is concentration-specific and tunable by varying $BiVO_4$ concentration. Thus, the present study provides the proof of concept that by tuning $BiVO_4$concentration in $BiVO_4$/ZnO dual layered photoanode, the solar to hydrogen efficiency can be significantly enhanced.

Figure 5.2 shows the linear sweep voltammetry of pure ZnO, pure $BiVO_4$ and $BiVO_4$-ZnO nanocomposites (B1, B2 and B3) samples. The photocurrent density observed to be 3.0 mA/cm^2 and 1.3 mA/cm^2 for sample B1 and ZnO, respectively at 0 V applied potential. The photocurrent is indicative of water oxidation efficiency. The higher slope of sample B1 indicates greater generation of charge carriers as compared to pure ZnO due to visible light driven photocatalytic activity of $BiVO_4$. Thus, sample B1 can be used for water splitting applications without any external bias. In sample B2 and B3, substantially lower photocurrent density is observed and onset of photocurrent density is only after applied bias voltage > 0.4 V and 0.6 V, respectively is due to the loss of majority of charge carriers due to surface recombination process, attributed to poor catalytic activity of $BiVO_4$. However, higher slope of graph indicate greater generation of charge carriers in sample B2 and B3 as compared to pure ZnO and sample B1, is attributed to higher concentration of $BiVO_4$. Thus, from voltammetry studies, it can be inferred that two competitive processes, carrier generation and carrier recombination are simultaneous taking place and both these processes increases with the increase of $BiVO_4$ concentration in $BiVO_4$/ZnO photoanode. In sample B2 and B3 carrier recombination process overweighs the carrier generation process resulting in lower photocurrent density with spike and overshoot features (supported by current vs time studies, Fig 5.1) and higher onset potential. Thus, to improve water-oxidation kinetics using dual layer $BiVO_4$/ZnO photoanode, optimization of $BiVO_4$ concentration is prerequisite so that it can successfully be used as a visible sensitizer or co-catalyst with rendered surface recombination process.

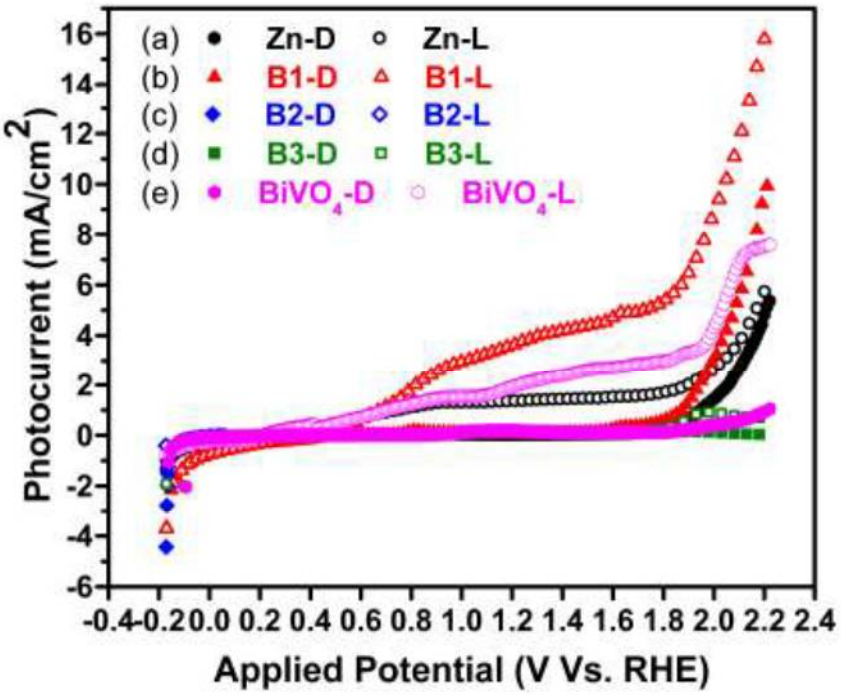

Figure 5.2 Photoelectrochemical properties (J vs V curve) of photoanode samples (a) pure ZnO (b) B1; $BiVO_4$ (0.035 M)/ZnO (c) B2; $BiVO_4$ (0.05 M)/ZnO and (d) B3; $BiVO_4$(0.1M)/ZnO in 1 M NaOH (scan rate, 50 mV/s). Light currents and dark currents are shown with respective solid and dashed color lines.

Electrochemical impedance measurements (EIS, Nyquist plots) were carried out to evaluate the charge transfer kinetics and performance of the working electrode of the sample ZnO, B1, B2 and B3. In the Nyquist curve, the high frequency curve correspond to solution resistance, mid frequency semicircular arc shows charge transfer resistance at solid electrolyte interface and low frequency tail correspond to diffusion. The data is recorded by applying a constant potential of 0.01 V and sweeping the frequency from 100000 to 0.1 Hz. By comparing all the graphs (fig. 5.3), it is clear that sample B1 has substantially small semi-circular arc in Nyquist plot; implying charge transfer resistance (R_{CT}) is lowest for sample B1 as compared to all other samples. Thus, contact resistance (R_{CT}) of the samples were in order of R_{CT} (B1) < R_{CT}(B3) < R_{CT} (B2) < R_{CT} (ZnO).

Thus, photoanode-electrolyte interface resistance is highest for pure ZnO, followed by sample B2, B3 and B1.

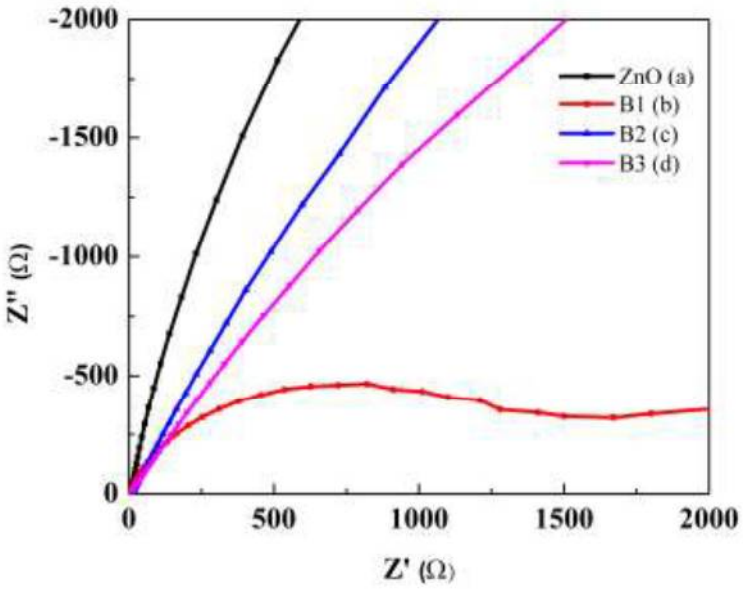

Figure 5.3. Electrochemical impedance Plots of photoanode samples (a) pure ZnO (b) B1; $BiVO_4$ (0.035 M)/ZnO (c) B2; $BiVO_4$ (0.05 M)/ZnO and (d) B3; $BiVO_4$ (0.1M)/ZnO

AC impedance (Electrochemical impedance) were recorded at constant frequency with step potential from -0.8 to +0 V and with the help of Mott-Schottky equation, we had plotted Mott-Schottky plots ($1/C^2$ vs applied potential). These curves were used to measure the carrier concentration and flat band potential on the basis of the Mott-Schottky equation. The Mott-Schottky plots of the samples are shown in the Figure 5.4. The plot and calculations are based on the following Mott-Schottky eq. given below:

Where, C (F) is the space-charge capacitance, A is the active geometric area, N_D (cm^{-3}) is the donor concentration, V is the applied voltage, k_B is the Boltzmann constant, T is the absolute temperature and e is the electric charge.

The slope ——— of the graph is used to calculate the carrier concentration (N_D) using the following equation:

—— ——

and intercept gives the flat band potential (V_{FB}). The decrease in slope signifies increase in donor carrier density and positive shift indicates increase in flat band potential summarizes the carrier concentration (N_D) and flat band potential (V_{FB}) for all the samples. The observed carrier concentration is in the order: N_D(B1) > N_D(ZnO) > N_D(B3) > N_D(B2). Thus, the carrier concentration is found to be maximum for sample B1. The increase in charge carrier concentration significantly impacts the photoelectrochemical properties. It shifts the Fermi level resulting in significant band bending leading to enhanced electric field in the space charge region that expedites the electron-hole separation in the space charge region. The flat band potential is a direct measure of the band bending. The V_{FB} was observed to increase from V_{FB} (B2) > V_{FB} (B1) > V_{FB} (B3)> V_{FB} ($BiVO_4$) > V_{FB} (ZnO). Additionally, the increase in charge carrier density indicates increase in conductivity of photo electrode. Thus, shift in V_{FB} is attributed to change in charge carrier concentration and change in Helmoltz layer potential [10].

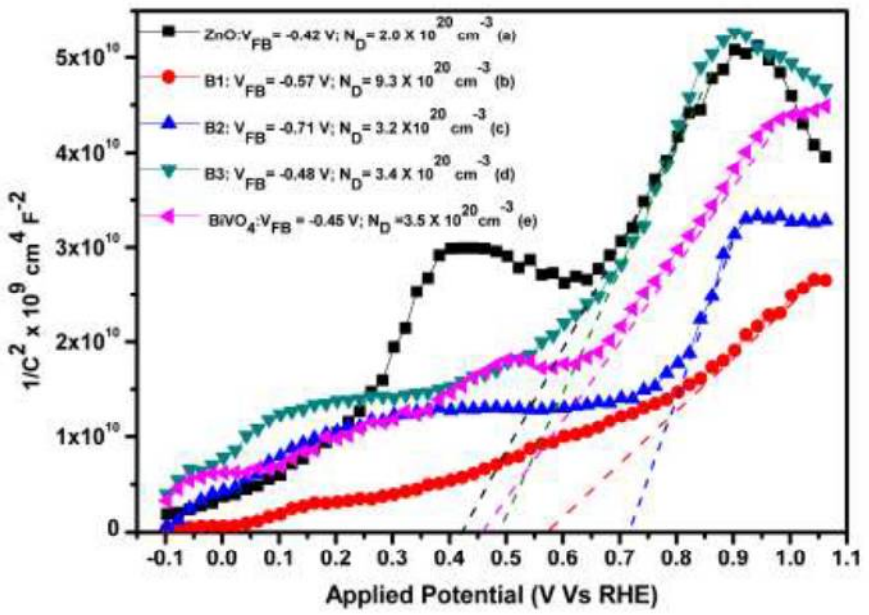

Figure 5.4 Mott-Schottky plots of photoanode samples (a) pure ZnO (b) B1;$BiVO_4$ (0.035 M)/ZnO (c) B2;$BiVO_4$ (0.05 M)/ZnO and (d) B3;$BiVO_4$ (0.1M)/ZnO (e) pure $BiVO_4$

5.3 Mechanism of action

The charge transfer mechanism in a multi-layered material for PEC depends on the band alignment type existing between two materials in the heterostructure i.e. $BiVO_4$ and ZnO here, suggesting that transfer of electrons from $BiVO_4$ to ZnO is possible and favorable.

The flat band potential (V_{FB}) of a semiconductor can give a good approximate of its band positions in an aqueous environment. Electrochemical impedance spectroscopy is a primary method to estimate V_{FB} which appears on the x-intercept of Mott-Schottky plot [217]. The values of V_{FB} for both ZnO and $BiVO_4$ lie within a broad range. In addition, this value can change as a function of pH by adsorption of OH- and H+ ions due to surface charging. For ex, V_{FB} for $BiVO_4$ has been determined to lie approximately between –0.7 and –0.3 V (vs Ag/AgCl) for pH varying from 5.8 to 7. Similarly, it lies between –0.29 V and +0.2 V (vs Ag/AgCl) for ZnO at pH 7.4 which clearly supports the fact that transfer of electrons from $BiVO_4$ to ZnO is feasible [218]. From our study,

V_{FB} was measured to be 0.66 and 0.70 V for pure ZnO and pure $BiVO_4$, which is slightly higher for $BiVO_4$. This suggests that band positions for both the materials are suitable for promoting the charge transfer from $BiVO_4$ to ZnO.

The complete picture of band positions for ZnO and $BiVO_4$ with PEC mechanism is presented by calculating their conduction band and valence band edge positions (Fig 5.5).

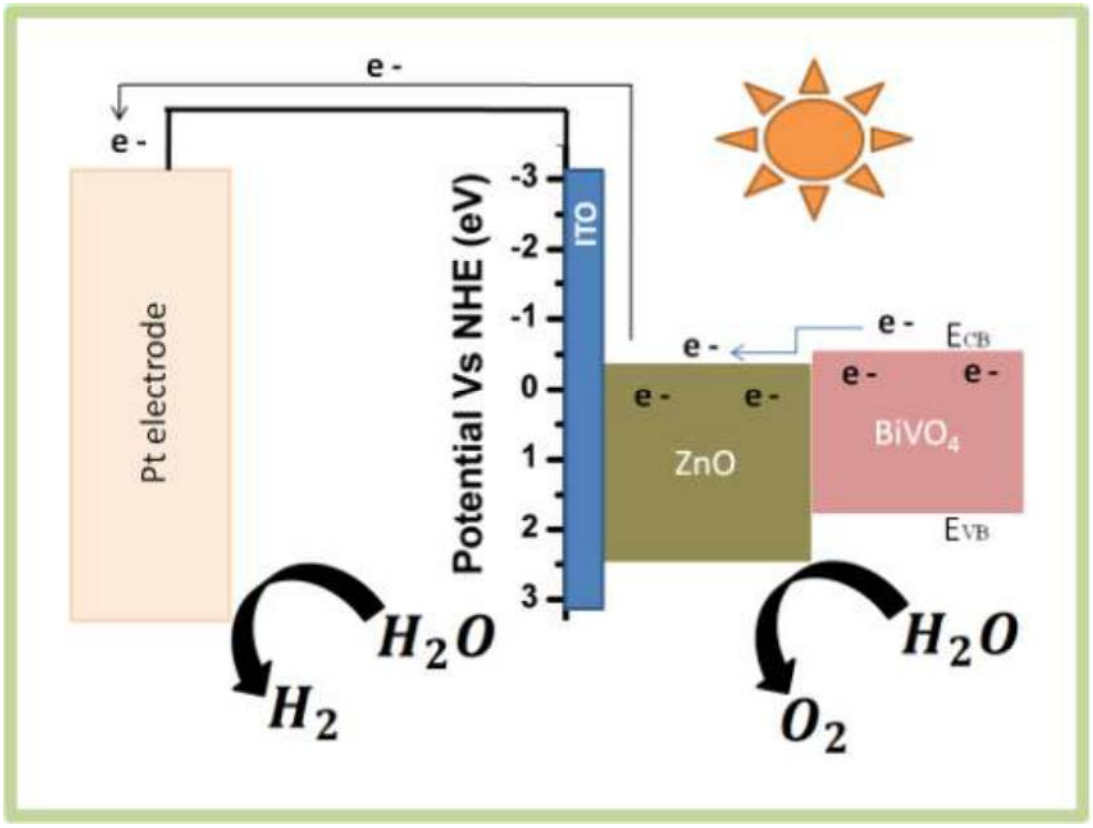

Fig 5.5. The schematic diagram to illustrate complete band diagram and PEC mechanism showing electron transfer from $BiVO_4$ (high CB edge material) to ZnO (low CB edge material) by almost matching flat band potential phenomenon.